



# Facile preparation of various ZnO nanostructures via ultrasonic mist vapor deposition: a systematic investigation about the effects of growth parameters

Hassan Alehdaghi<sup>1</sup> · Mohammad Zirak<sup>1</sup>

Received: 7 September 2018 / Accepted: 10 December 2018 / Published online: 2 January 2019  
© Springer Science+Business Media, LLC, part of Springer Nature 2019

## Abstract

ZnO thin films with various surface morphologies were deposited on glass substrate via a facile and well-controllable method so-called ultrasonic mist vapor deposition (UMVD). The effects of important growth parameters namely substrate temperature ( $T_s$ ), nozzle-substrate distance ( $D$ ) and nozzle aperture diameter ( $d$ ) on optical, electrical and surface properties (both in micro and macro-scale) of synthesized thin films were carefully investigated. In case of  $d = 10$  mm and  $D = 6$  cm, ZnO nanoseeds and nanorods were grown at  $T_s = 330$  and  $500$  °C, respectively. Interestingly, ZnO nanosheets were grown perpendicular to the substrate when  $d = 10$  mm,  $D = 9$  cm and  $T_s = 400$  °C. More rough surfaces (in macroscopic scale) were grown for small  $D$  (6 and 9 cm) and lower substrate temperature ( $T_s = 330$  and  $400$  °C) while for  $T_s = 500$  °C a smooth and uniform surface can be obtained at any distance. The layer prepared with  $d = 10$  mm, has the lowest roughness (33 nm) which is one order of magnitude lower than other samples. Increment of  $T_s$ ,  $d$  and also  $D$  reduced the electrical sheet resistance. The growth mechanisms leading to obtain various morphologies for different samples were also proposed and discussed.

## 1 Introduction

Zinc oxide is a semiconductor (SC) with a direct band gap of 3.3 eV and an exciton binding energy of around 60 meV [1, 2]. As a SC, ZnO has high electron mobility (higher than famous  $\text{TiO}_2$  semiconductor [3]), high transparency and photoluminescence properties as same as CdS quantum dots [4, 5]. Moreover, among all SCs, zinc oxide has the most diverse nanostructures including nanowires (NWs) [6], nanorods (NRs) [7], nanosheets (NSs) [8], nanobelts (NBs) [9], nanotubes (NTs) [10], nanoflowers (NFs) [11] and etc. These various nanostructures possess different optical and physical properties making them suitable as building blocks for diverse devices. Therefore, ZnO is an important multifunctional material which can be used in a wide range of applications such as solar cells [12, 13], light emitting diodes (LEDs) [14–17], sensors [18], transparent conductive films [19, 20] and photocatalytic applications [21–23].

The properties of nanostructured ZnO thin films strongly depend on their preparation procedures [24]. Over the past decades, numerous physical and chemical methods such as pulsed laser deposition (PLD) [25, 26], molecular beam epitaxy (MBE) [27], sputtering deposition [28], chemical vapor deposition (CVD) [29, 30], hydro/solvothermal method [31, 32], sol-gel [33, 34], ultrasonic spray pyrolysis (USP) [35, 36] and etc. have been developed to prepare different ZnO nanostructures with desired physico-chemical properties. ZnO nanostructured thin films with high quality, high charge carrier mobility and desired uniformity can be obtained via physical methods of MBE, PLD, sputtering and so on. But, these methods need expensive and complicated equipment which are not feasible in many common labs. In this regard, chemical methods (hydro/solvothermal, sol-gel, USP and etc.) have great advantages of low-cost and simple setups that if the process parameters are adequately tuned and controlled, high quality thin films could be also prepared.

Sol-gel method (using spin coating or dip coating deposition technique) is most common facile chemical route to prepare diverse ZnO nanostructured thin films. But, this approach is not compatible with uniform and large scale thin film preparation with unlimited thickness. Furthermore, it is not possible to completely remove some residual organic compounds such as ethanalamine (EA) which are commonly used in sol gel

✉ Mohammad Zirak  
m.zirak@hsu.ac.ir

<sup>1</sup> Department of Physics, Hakim Sabzevari University, 9617976487, Sabzevar, Islamic Republic of Iran

based techniques [37]. These residues have significant effects on the properties of prepared thin films. Ultrasonic mist vapor deposition (UMVD) is a simple chemical technique to deposit small as well as large area ZnO thin films with desired thickness at low cost without using any additive compound [37–39].

In UMVD technique, a metal source solution (usually with low viscosity) is ultrasonically atomized to produce mist particles or aerosols. The atomized particles are transferred via a carrier gas toward a pre-heated substrate to be deposited as a film [40]. All of these non-vacuum steps are conducted under ambient pressure and there is no need to a high pressure carrier gas tank or pump, which are used in common spray pyrolysis technique. Moreover, in UMVD, all of the important deposition parameters such as mist flow rate, substrate temperature and alignment, nozzle diameter, nozzle to substrate distance, spraying geometry and thin film thickness can be easily and adequately controlled. Thus UMVD can eliminate many drawbacks of sol–gel method.

In order to improve the physical properties of ZnO nanostructured thin films prepared via UMVD, all of important growth parameters should be investigated and optimized. Although there are numerous reports about sprayed ZnO films [35, 41, 42], there is still lack of a comprehensive investigation about the effect of important growth parameters on topographical, optical and electrical properties of the prepared thin films. Especially, there are limited reports about the effects of these parameters on the growth of various nanostructures.

Herein, we have manipulated the important process parameters of UMVD namely substrate temperature ( $T_s$ ), nozzle diameter ( $d$ ), nozzle–substrate distance ( $D$ ). The effects of these parameters on surface topographies and morphologies as well as optical and electrical properties of prepared ZnO thin films were explored in a systematic manner both in microscopic and macroscopic scale. We found that uniform ZnO thin film with various morphologies including nanoseeds, nanorod, nanoball, nanosheets or a mixture of them can be obtained by appropriate selection of the mentioned growth parameters. Finally, the mechanisms responsible for such obtained morphologies were also proposed and discussed based on characterization results. Our findings provide very valuable information for various ZnO thin film applications and strongly verify the high advantages of our applied method to prepare different desired ZnO nanostructures with high accuracy in a well controllable and straightforward manner.

## 2 Experimental

### 2.1 Materials

Zinc acetate ( $\text{Zn}(\text{CH}_3\text{COO})_2\cdot\text{H}_2\text{O}$ , analytical reagent grade, Merck) was used as received without further purification.

The precursor solution with concentration of 50 mM was obtained by dissolving appropriate amount of zinc acetate in 500 mL of deionized (DI) water. Few drops of acetic acid were added to get a clear solution. The used substrates were soda lime glasses with dimensions of  $1.3 \times 1.3$  cm. Before deposition, the substrates were cleaned via sonication in acetone (10 min) and then ethanol (10 min) and finally methanol (10 min) in an ultrasonic bath.

### 2.2 Thin film deposition

The zinc oxide thin films were deposited via a home-made UMVD system. The precursor solution was put inside a Teflon-lined cylinder equipped with a mini industrial piezoelectric crystal with operational frequency of 1.7 MHz which was used as ultrasonic transducer to produce mist vapor. The air was used as carrier gas at atmospheric condition to produce a mist vapor production rate of 5 mL/min. The mist vapor flowed through a nozzle placed normal to the glass substrates. The distances of nozzle to the substrates ( $D$ ) were chosen as 6, 9 and 12 cm. The different nozzle aperture diameters ( $d$ ) of 6, 7, 8 and 10 mm were also considered. The effect of substrate temperature ( $T_s$ ) was also investigated by setting the hot plate temperature at 330, 400, 450 and 500 °C. Figure 1 shows a schematic illustration of used UMVD system.

### 2.3 Characterization

The surface morphologies of ZnO nanostructured thin films were studied by a field emission scanning electron microscopy (FE-SEM, TESCAN Mira 3-XMU). A Jasco V530 UV–Vis spectrophotometer was utilized to investigate the optical properties of the prepared samples. The crystal phase of the layers was determined via X-ray diffraction technique (XRD, PANalytical X'Pert PRO MPD,  $\text{CuK}_\alpha$  irradiation,  $\lambda = 1.54 \text{ \AA}$ ) with a step of  $0.03^\circ$ . The macroscopic surface topographies were evaluated via a confocal microscope (Nanofocus) with lateral resolution ( $X$ – $Y$  plane) of  $1 \mu\text{m}$  and vertical resolution ( $Z$  axis) of 1 nm. The electrical properties of the thin films were characterized via Keithley 2400 power supply and a four-point probe system.

## 3 Results and discussions

The XRD pattern of ZnO thin film grown with  $T_s = 500^\circ\text{C}$ ,  $D = 6$  cm and  $d = 10$  mm can be seen in Fig. 2. As it is clear, there are five sharp peaks at  $2\theta = 34.49, 36.28, 47.55, 62.88$  and  $67.90$  degree corresponding to crystal planes of (002), (101), (102) (103) and (112) respectively. This XRD pattern corresponds to ZnO wurtzite crystal structure according to JCPDS card number of 036-1451 [43]. The very sharp peak

**Fig. 1** Schematic illustration of home-made UMVD system used to prepare ZnO thin films

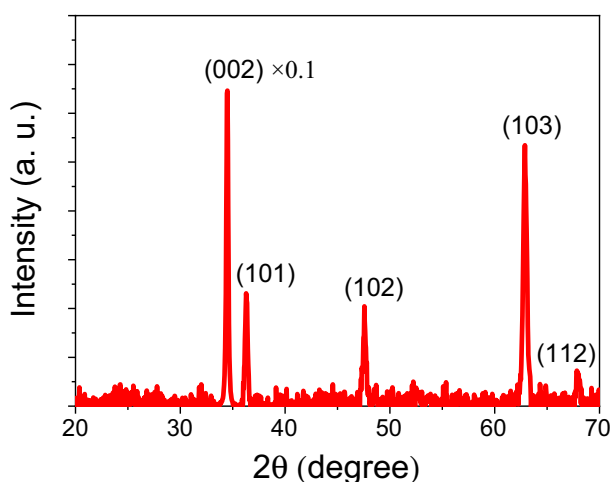
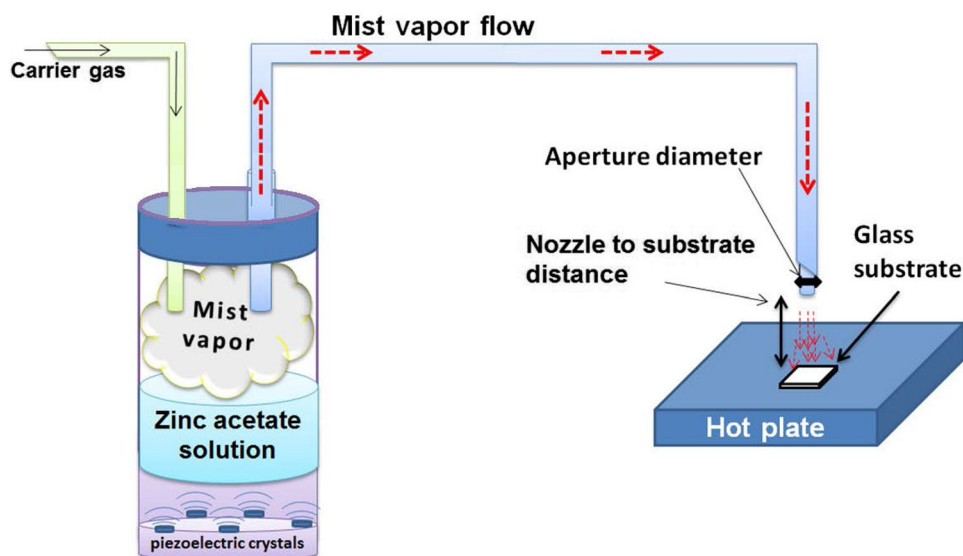


**Fig. 2** XRD pattern of ZnO thin film grown at  $D=6$  cm,  $T_s=500$  °C and  $d=10$  mm. the intensity of (002) peak has been divided by 10 for better demonstration

at  $2\theta=34.49^\circ$ , corresponding to (002) plane, indicates the tendency of ZnO crystal to grow vertical to the substrate. It has been established that the high temperature difference between the hot spots (produced by ultrasonic waves due to acoustic cavitation followed by impulsive collapse) and the bulk solution could be responsible for the preferential (002) crystal orientation [24, 44]. The obtained XRD data are in agreement with other reports [35, 45]. The crystallite size of the prepared sample was determined by Debye–Scherrer equation:

$$S = \frac{0.9\lambda}{\beta \cos \theta} \quad (1)$$

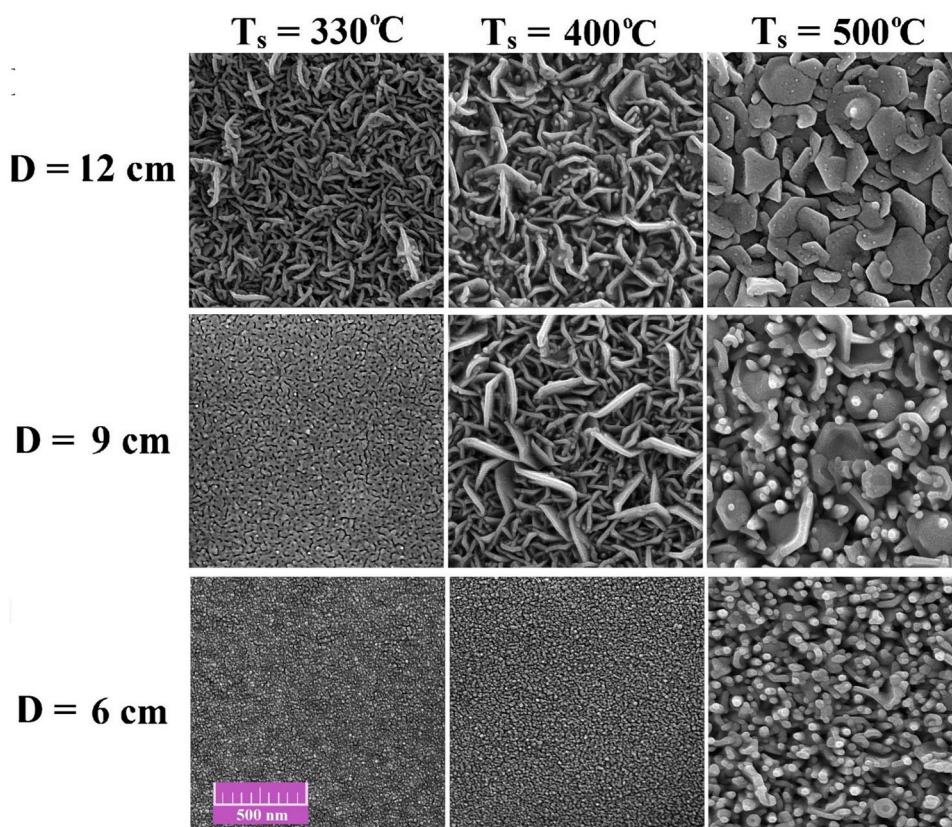
where  $S$  is the crystal size,  $\lambda$  is X-ray wavelength (0.154 nm),  $\beta$  is full width at half-maximum (FWHM, radian) and  $\theta$

is diffraction angle. Considering (002) diffraction peak ( $\theta=17.245^\circ$ ), the  $S \approx 36$  nm was obtained for deposited ZnO crystal.

The SEM images of ZnO thin films prepared at different  $D$  and  $T_s$  have been shown in Fig. 3. In case of  $D=6$  cm, it can be seen that ZnO nanoseeds were grown with average diameter of 10.1 nm and 12.5 nm for  $T_s=330$  and 400 °C, respectively. While for the sample deposited at  $T_s=500$  °C, seeds were changed to nanorods with average diameter of 40 nm, in good agreement with crystal size ( $S$ ) obtained via XRD results. The results are obviously different for  $D=9$  cm. A smooth worm-like morphology can be seen at  $T_s=330$  °C, while for  $T_s=400$  °C, nanosheets with average size of 150 nm and thickness of 15 nm were grown perpendicular to the substrate. By increasing the  $T_s$  to 500 °C, a mixed vertical nanosheet–nanorod morphology was observed. For  $D=12$  cm, the rough worm-like morphology, vertical nanosheet and semi-hexagonal petals (with diagonal of 250 nm) were grown at  $T_s=330$ , 400 and 500 °C, respectively. As it is clear from Fig. 3, both  $T_s$  and  $D$  have significant effects on morphologies of deposited ZnO thin films. The Various structures, from smooth seed layers to complex mixed nanorod–nanosheet morphology, could be obtained easily by changing the nozzle to substrate distance as well as substrate temperature which can be controlled with high accuracy.

The effects of growth parameters on macro-scale topography of the prepared samples were studied by confocal microscopy. The obtained 3D images have been sorted in Fig. 4, same as the SEM images order. The images were taken from selected areas with lateral dimensions of  $270 \times 270$   $\mu\text{m}$ . Herein, it can be seen that with increasing the distance (down to up in the figure) layers with smoother surface were grown. For short  $D$ , the mist vapor drops do

**Fig. 3** SEM images of ZnO thin films deposited with different  $D$  and  $T_s$ . the “ $d$ ” was 10 mm for all samples



not have enough time to evaporate before reaching to surface leading to increase of surface roughness [46, 47].

Similar behavior can also be observed when  $T_s$  was increased. Substrate temperature increment leads to faster drying of solution drops and they completely evaporate before reaching the samples surfaces [47, 48]. Therefore, a thin film with smoother surface could be obtained. As Fig. 4 shows, the best surface macro-uniformity was obtained when  $D = 12$  cm and  $T_s = 500$  °C. The obtained macro-roughness data for different sample have been listed in Table 1. It is worth to note that for distance of  $D = 12$  cm and nozzle diameter of  $d = 10$  mm, the diameter of mist flow at substrate surface was 2 cm, which is larger than the substrate dimensions ( $1.3 \times 1.3$  cm). Therefore, it is possible to achieve uniform deposition by  $D = 12$  cm. The uniformity of the samples obtained by  $D = 12$  cm and  $d = 10$  mm, was confirmed via confocal microscope images captured from different areas of the samples surfaces.

To study optical properties of the samples prepared with different growth conditions, transmittance spectra of the samples were recorded with UV–Visible spectrometer. Figure 5 shows the effects of temperature and distance on the optical properties of the samples. All of the samples show the same absorption edge at 375 nm, corresponding to band gap energy ( $E_g$ ) of 3.31 eV, which is in good agreement with standard ZnO absorption edge and band gap energy

[31, 49]. In the top row of Fig. 5, three sets of UV–visible transmittance spectra have been plotted for  $T_s = 330$ , 400 and 500 °C (Fig. 5a, b, c, respectively) and inside every plot of this set, the effect of distance has been compared. At  $T_s = 330$  °C (Fig. 5a), it can be seen some peaks and valleys in range of 400–1100 nm when  $D = 12$  cm, while there is no peak or valley when  $D = 6$  and 9 cm. The similar behavior can also be observed when the thin films are prepared at  $T_s = 400$  °C (Fig. 5b). The presence of such fluctuations in transmittance spectrum is a result of light interference from compact and smooth surfaces [38]. Therefore, the behavior observed in transmittance spectra indicates that more rough surfaces (in macroscopic scale) were grown for short  $D$  (6 and 9 cm) and lower substrate temperature ( $T_s = 330$  and 400 °C) while the sample prepared at  $D = 12$  cm is more uniform with low roughness. When  $T_s$  increased to 500 °C, all of the layers showed some peaks and valleys in their transmittance spectra (Fig. 5c), indicating that a smooth and uniform surface can be obtained at any distance at high substrate temperature.

In order to observe the effect of temperature on the optical properties of the layers, three sets of curves have been depicted in the bottom row of Fig. 5(d–f) corresponding to  $D = 6$ , 9 and 12 cm. Inside every set, there are three curves related to  $T_s = 330$ , 400 and 500 °C. Using such ordering and comparison, it can be seen that for small  $D$  values (6 and



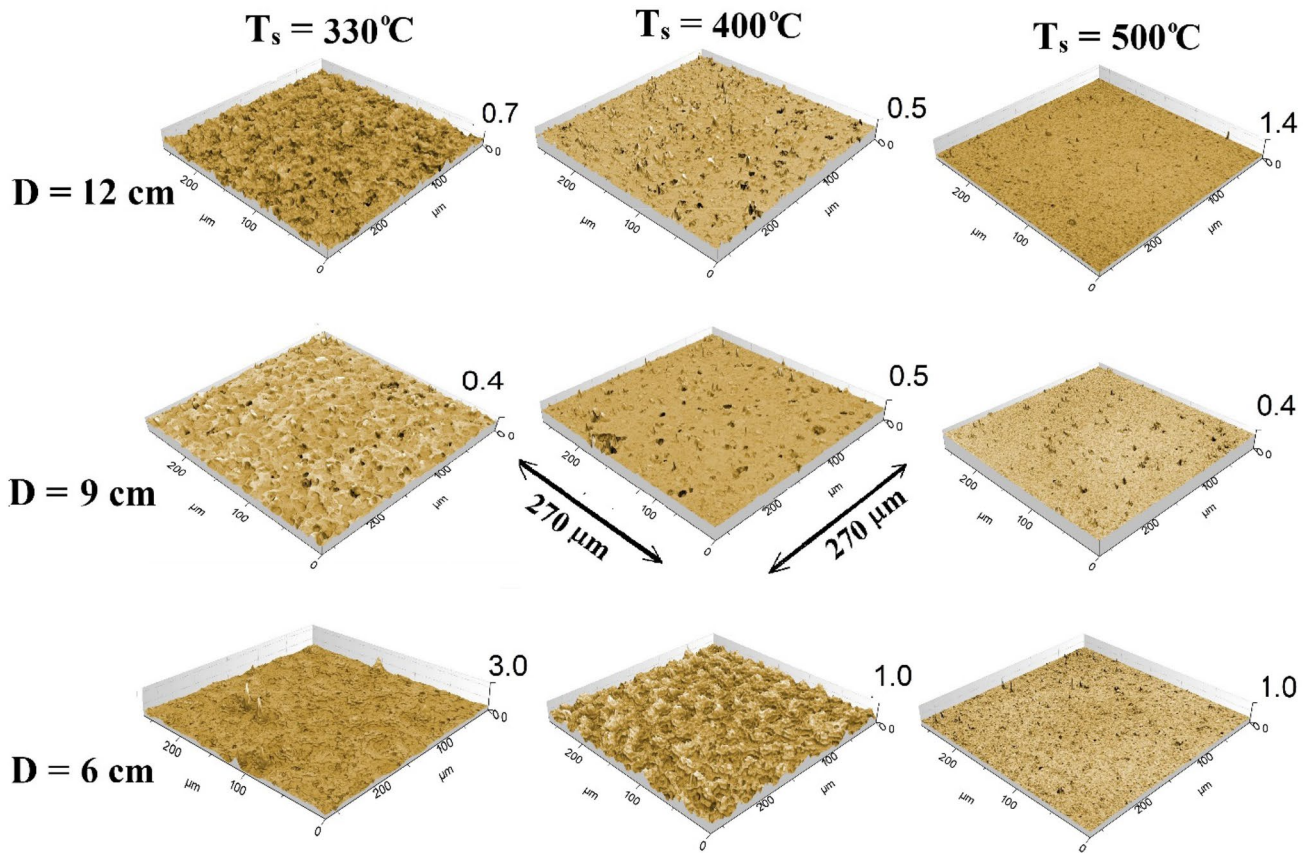


**Fig. 4** 3D Confocal microscope images of ZnO thin films deposited with  $d=10$  mm and different substrate temperatures and nozzle–substrate distances. All numbers in images have  $\mu\text{m}$  unit

9 cm) only high  $T_s$  could result in a transmission spectrum with fluctuations which is originated from a smooth and compact layer. But for long  $D$  (12 cm), a layer with low roughness could be obtained even at low  $T_s$ . The results obtained from UV–visible (Fig. 5) are completely in agreement with confocal microscope images and data (Fig. 4; Table 1). These findings provide very valuable information for various ZnO thin film applications. For instance, if a ZnO thin film with smooth surface should be deposited at low temperature (in case of organic substrate for example) one should select high nozzle to substrate distance.

$T_s$  and  $D$  have also significant effects on sheet resistance ( $R_s$ ) and deposition time ( $t_d$ ) (to get a specific thickness of 300 nm). Figure 6 provides a comprehensive view which shows three dimensional bars comparing the effects of substrate temperature and nozzle-substrate distance on  $t_d$ ,  $R_s$  and surface roughness. It is clear from Fig. 6(a) that longer deposition time is needed as  $D$  is increased for every substrate temperature. In another view of point,  $t_d$  increased as  $T_s$  is higher for every nozzle-substrate distance. Higher  $T_s$  causes more evaporation of solution drops reaching to the surface. Similarly, for longer distances, there is more time for drops to reach to the substrate leading to more

evaporation. Therefore, longer  $t_d$  will be needed as  $T_s$  and  $D$  increase.

Figure 6(b) and (c) show that  $D$  and  $T_s$  have influenced on the surface roughness (obtained from confocal microscope) and sheet resistance in a same manner. It can be concluded that increment of both  $T_s$  and  $D$  has resulted in surface roughness reduction as well as  $R_s$ . Higher  $T_s$  results in lower deposition rate and therefore smoother layer with lower surface roughness could be obtained. Such a smooth layer with less pinholes and defects has lower  $R_s$ .

The maximum value that our equipment could measure was about  $1000 \text{ M}\Omega/\square$ , so for two samples that deposited at  $330^\circ\text{C}$  in  $D=6$  and  $9$  cm, our data for  $R_s$  are overflow. Due to absence of any doping in ZnO lattice, the resistance of layers was fairly high. It is clear that the  $R_s$  and surface roughness behavior of the samples presented in Fig. 6 are in good consistency with optical properties obtained from UV–visible transmittance data (Fig. 5).

After investigation of  $T_s$  and  $D$  effects on ZnO thin films, the effect of nozzle diameter ( $d$ ) was also explored. To do that, three different nozzle diameters of 6, 7, 8 and 10 mm were considered. The substrate temperature and nozzle–substrate distance were fixed at  $450^\circ\text{C}$  and 9 cm,

**Table 1** The effects of substrate–nozzle distance and substrate temperature on physical properties of ZnO thin films deposited via UMVD technique. The data were obtained for nozzle diameter of  $d = 10$  mm

	$T_s$ (°C)	D (cm)	$t_d$ (s)	Roughness $\pm 5\%$ (nm)	Resist- ance $\pm 5\%$ ( $M\Omega/\square$ )
Substrate–nozzle Distance (D)	330	6	110	165	> 1000
		9	245	72	> 1000
		12	900	37	400
	400	6	210	130	850
		9	300	77	260
		12	1080	26	180
	500	6	220	15	225
		9	590	21	215
		12	1440	12	145
	D (cm)	$T_s$ (°C)	$t_d$ (s)	Roughness $\pm 5\%$ (nm)	Resist- ance $\pm 5\%$ ( $M\Omega/\square$ )
Substrate temperature ( $T_s$ )	6	330	110	166	> 1000
		400	210	130	850
		500	220	15	225
	9	330	245	72	> 1000
		400	260	68	32
		500	590	21	43
	12	330	900	37	80
		400	1080	26	26
		500	1440	12	29

respectively. The effect of nozzle diameter on the optical and surface properties of prepared ZnO thin films has been shown in Fig. 7 for different samples. According to Fig. 7c, there is no fluctuation in transmittance spectra except for the layer prepared with  $d = 10$  mm. other nozzle diameters cannot provide a smooth and compact layer (in macro-scale). This fact was also confirmed via confocal microscope data (Fig. 7b; Table 1). As it is clear from Fig. 7b, the layer prepared with  $d = 10$  mm, has the smoothest surface with lowest roughness which is one order of magnitude lower than other samples. From micro-scale view of point, The SEM images were taken from the thin films prepared with different “ $d$ ” and the results have been shown in Fig. 7a. Accordingly, the size of ZnO seeds on the surface increased, and seeds coalesce together to make worm-like shapes as nozzle diameter increased from 6 to 8 mm. furtherer increase of “ $d$ ” to 10 mm, makes worm-like seeds to grow vertical to the substrate and nanosheets were formed. As it is mentioned in Table 2, the deposition time is prolonged by increasing nozzle diameter and thus the seeds have more time to coalesce and grow vertical to the substrate.

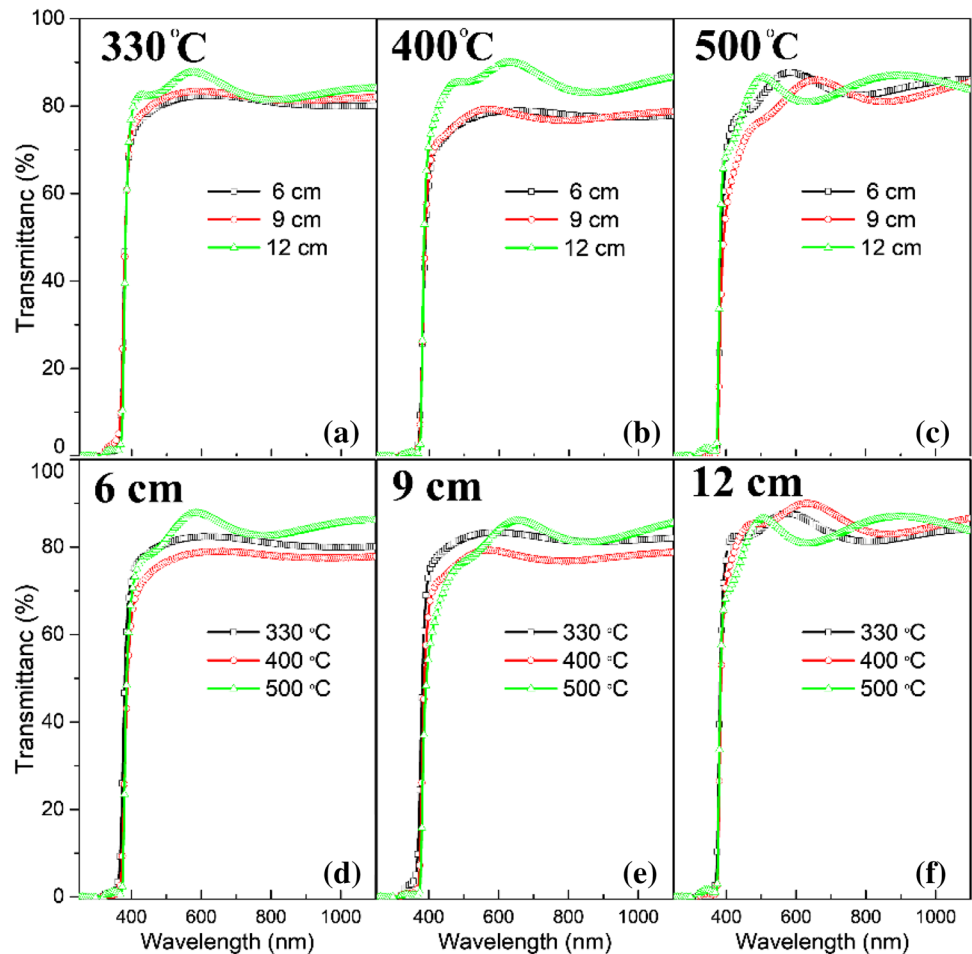
The information about the different ZnO thin films deposited with various nozzle diameters has been listed in Table 2.

### 3.1 Growth mechanism

After considering all of the obtained results, the growth mechanism of ZnO thin films for different  $T_s$  and D could be proposed as illustrated schematically in Fig. 8. In case of small D values (Fig. 8a), the solution droplets quickly reach to the hot substrate and have not enough time to evaporate before deposition. Therefore, big mist particles drop down to the substrate surface and create island-like particles (Fig. 8a). Solvent evaporation through such big and fixed islands results in splitting them into many small ZnO particles (seeds) with a lot of voids among them [47, 48], leading to a seeded surface morphology with high macroscopic surface roughness. Now, if the substrate temperature is high, these seeds can migrate through the surface more easily and coalesce together to grow up and fill the voids because of incorporative principle of Ostwald [39, 50]. Therefore, a compact smooth layer would be obtained with low macroscopic surface roughness. Dense ZnO seeds provide growth nuclei along the direction of which has the lowest energy in wurtzite crystal structure [39, 51]. Afterward, the more growth of ZnO will be along (002) crystal plane which results in vertically grown nanorods.

When a large D value is selected (Fig. 8b), the solution droplets have enough time to evaporate as they approach to

**Fig. 5** UV–visible spectra of ZnO thin films prepared via UMVD with  $d = 10$  mm and different  $D$  and  $T_s$ . The top row presents the effect of  $D$  at constant  $T_s$  and bottom row depicts vice versa



the substrate. Such pre-deposition evaporation lead to gas-phase diffusion onto the substrate which allows the precursor gases to make chains on the surface [46, 47]. The growth of these chains upon low and mild heating provides worm-like surface morphology. But if the  $T_s$  is high, the chains can migrate and agglomerate together laterally to create nanoplates. The mentioned mechanism can be also responsible for seed and worm-like morphologies observed for the ZnO thin films prepared with different nozzle diameter.

## 4 Conclusion

A systematic investigation was performed to explore the effects of growth parameters on optical, electrical and surface properties of ZnO thin films deposited via a facile atmospheric pressure ultrasonic mist vapor deposition. Many different morphologies, including nanoseeds, nanosheets and mixed nanorod–nanosheets morphologies, were obtained by selecting different substrate–nozzle distance ( $D$ ), substrate temperature ( $T_s$ ) and nozzle diameter ( $d$ ). The results showed that increment of both  $T_s$  and  $D$  has reduced surface roughness as well as  $R_s$ . A smooth and compact layer (in macro-scale) was obtained using large nozzle diameter ( $d = 10$  mm) which was confirmed via confocal microscope and UV–visible transmittance data. The mechanisms of the observed behavior of the samples were also proposed and discussed. These parameters ( $D$ ,  $T_s$  and  $d$ ) are easily controllable with high accuracy and straightforward manner to prepare different desired ZnO surface structures.

**Fig. 6** Three dimensional plots of deposition time (a), surface roughness (b) and sheet resistance (c) obtained for the ZnO thin films deposited at different substrate temperature and nozzle-substrate distance

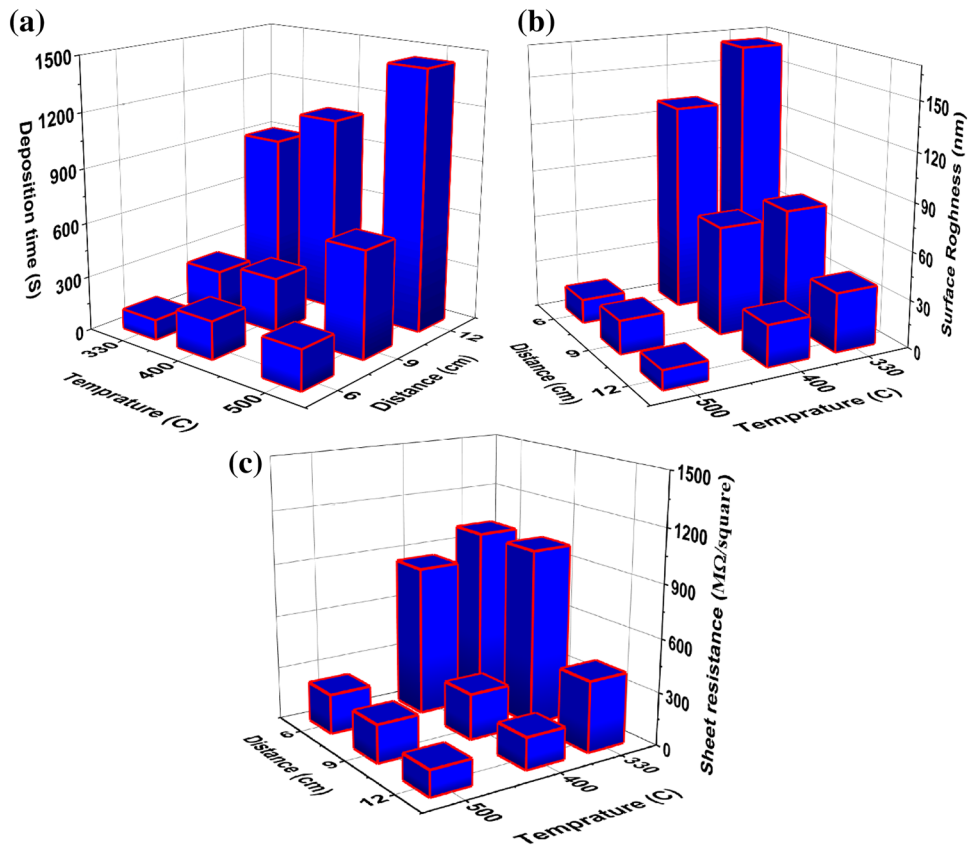


**Fig. 7** Effect of nozzle diameter on the surface properties in microscale a SEM images, macro-scale b confocal microscope images and optical properties c UV–visible transmittance spectra. All the layers were deposited at  $T_s = 450\text{ }^\circ\text{C}$  and  $D = 9\text{ cm}$

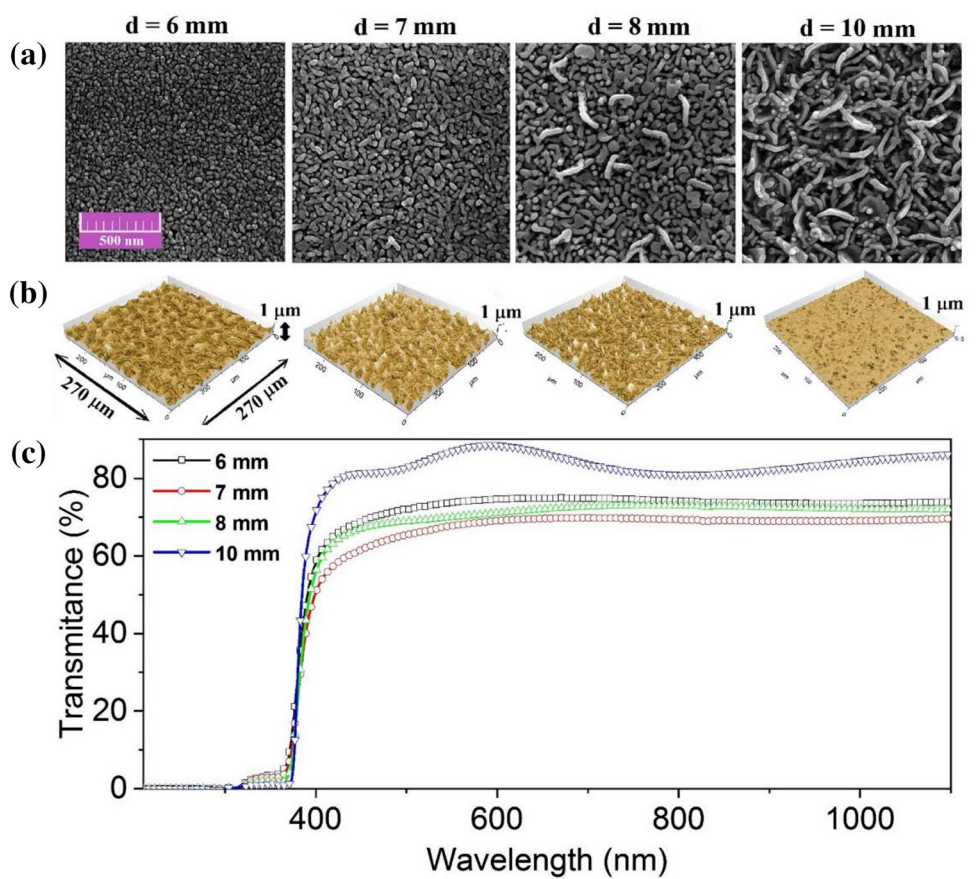




**Table 2** The effect of nozzle diameter on physical properties of ZnO thin films deposited via UMVD technique. The data were obtained at  $T_s = 450\text{ }^\circ\text{C}$  and  $D = 9\text{ cm}$

Nozzle Diameter (d) (mm)	$t_d$ (s)	Roughness $\pm 5\%$ (nm)	Sheet Resistance $\pm 5\%$ ( $\text{M}\Omega/\square$ )
6	51	140	175
7	72	156	150
8	140	136	128
10	300	33	18

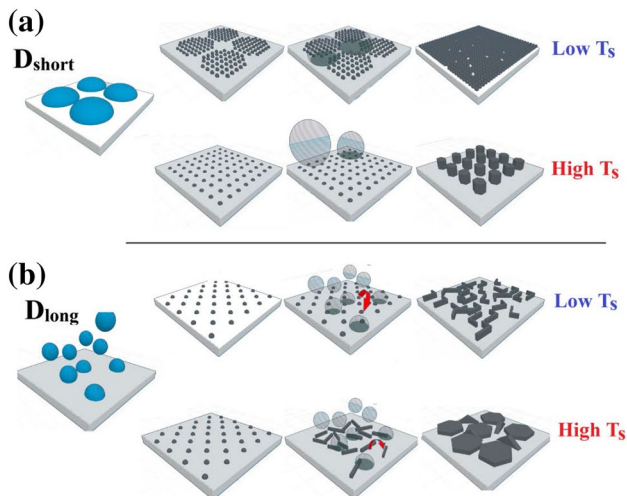


**Fig. 8** Schematic illustration of proposed growth mechanism for ZnO thin films prepared via UMVD under different growth parameters

**Acknowledgements** The Authors would like to thank Research and Technology Council of the Hakim Sabzevari University for financial support.

## References

1. A. Ouhaibi, M. Ghamnia, M.A. Dahamni, V. Heresanu, C. Fauquet, D. Tonneau, *J. Sci. Adv. Mater. Devices* **3**(1), 29 (2018)
2. M. Samadi, M. Zirak, A. Naseri, E. Khorashadizade, A.Z. Moshfegh, *Thin Solid Films* **605**, 2 (2016)
3. S. Vanalakar, R. Pawar, M. Suryawanshi, S. Mali, D. Dalavi, A. Moholkar, K. Sim, Y. Kwon, J. Kim, P. Patil, *Mater. Lett.* **65**(3), 548 (2011)
4. H. Alehdaghi, M. Marandi, M. Molaei, A. Irajizad, N. Taghavinia, *J. Alloy. Compd.* **586**, 380 (2014)
5. M. Cui, Z. Zhang, Y. Wang, A. Finch, P. Townsend, *Luminescence* **33**(4), 654 (2018)
6. V. Errico, G. Arrabito, E. Fornetti, C. Fuoco, S. Testa, G. Saggio, S. Rufini, S. Cannata, A. Desideri, C. Falconi, *ACS Appl. Mater. Interfaces* **10**(16), 14097 (2018)
7. X. Li, S. Liu, K. Fan, Z. Liu, B. Song, J. Yu, *Adv. Energy Mater.* **8**(18), 1800101 (2018)
8. H. Mou, C. Song, Y. Zhou, B. Zhang, D. Wang, *Appl. Catal. B* **221**, 565 (2018)

9. G. Li, Y. Su, Y.-Y. Li, Y.-X. Li, Z. Guo, X.-J. Huang, J.-H. Liu, *Nanotechnology* **29**(44), 445501 (2018)
10. H. Oh, J. Park, W. Choi, H. Kim, Y. Tchoe, A. Agrawal, G.C. Yi, *Small* **14**(17), 1800240 (2018)
11. L. Shi, D. Li, J. Yu, H.-M. Zhang, S. Ullah, B. Yang, C. Li, C. Zhu, J. Xu, *J. Power Sources* **387**, 64 (2018)
12. P. Mbule, D. Wang, R. Grieseler, P. Schaaf, B. Muhsin, H. Hoppe, B. Mothudi, M. Dhlamini, *Sol. Energy* **172**, 219 (2018)
13. Z. Zang, *Appl. Phys. Lett.* **112**(4), 042106 (2018)
14. F. Jiang, J. Chen, H. Bi, L. Li, W. Jing, J. Zhang, J. Dai, R. Che, C. Chen, Y. Gao, *Appl. Phys. Lett.* **112**(3), 033505 (2018)
15. M.-C. Tseng, D.-S. Wu, C.-L. Chen, H.-Y. Lee, R.-H. Horng, *Appl. Surf. Sci.* **432**, 196 (2018)
16. H. Alehdaghi, M. Marandi, A. Irajizad, N. Taghavinia, *Org. Electron.* **16**, 87 (2015)
17. H. Chun-Ying, H. Fu-Fan, W. Chia-Ling, C. Ming-Liang, T. Ping-Hung, T. Sian-Rong, Y. Ting-Wei, L. Ya-Ju, *Appl. Phys. Express* **11**(7), 075103 (2018)
18. S.A. Alavi-Tabari, M.A. Khalilzadeh, H. Karimi-Maleh, *J. Electroanal. Chem.* **811**, 84 (2018)
19. C.-Y. Tsay, K.-C. Pai, *Thin Solid Films* **654**, 11 (2018)
20. H. Kang, Z. Lu, Z. Zhong, J. Gu, *Mater. Lett.* **215**, 102 (2018)
21. V. Vaiano, M. Matarangolo, J. Murcia, H. Rojas, J. Navío, M. Hidalgo, *Appl. Catal. B* **225**, 197 (2018)
22. S. Bazazi, N. Arsalani, A. Khataee, A.G. Tabrizi, *J. Ind. Eng. Chem.* **62**, 265 (2018)
23. M. Zirak, O. Moradlou, M.R. Bayati, Y.T. Nien, A.Z. Moshfegh, *Appl. Surf. Sci.* **273**, 391 (2013)
24. O. Dimitrov, D. Nesheva, V. Blaskov, I. Stambolova, S. Vassilev, Z. Levi, V. Tonchev, *Mater. Chem. Phys.* **148**(3), 712 (2014)
25. J.A.G. de León, J.G.Q. Galvan, A.P. Centeno, G.G. Rosas, E. Camps, M.A. Santana-Aranda, *Mater. Res. Express* **5**(6), 066417 (2018)
26. W. Shaojun, J. Lan, H. Weina, H. Jie, L. Xiaowei, W. Qingsong, L. Yongfeng, *Appl. Phys. Express* **11**(5), 052703 (2018)
27. O.W. Kennedy, M.L. Coke, E.R. White, M.S. Shaffer, P.A. Warburton, *Mater. Lett.* **212**, 51 (2018)
28. H. Makino, H. Shimizu, *Appl. Surf. Sci.* **439**, 839–844 (2018)
29. M.M. Reddy, G.R. Reddy, K. Chennakesavulu, E. Sundaravadiel, S. Prasath, A. Rabel, J. Sreeramulu, *J. Porous Mater.* **24**(1), 149 (2017)
30. M. Thomson, J. Hodgkinson, D. Sheel, *Surf. Coat. Technol.* **230**, 190 (2013)
31. M. Zirak, O. Akhavan, O. Moradlou, Y.T. Nien, A.Z. Moshfegh, *J. Alloy. Compd.* **590**, 507 (2014)
32. X. San, M. Li, D. Liu, G. Wang, Y. Shen, D. Meng, F. Meng, *J. Alloy. Compd.* **739**, 260 (2018)
33. W. Shin, W. Cho, S.J. Baik, *Mater. Res. Express* **5**, 1 (2018)
34. M. Arif, A. Sanger, P.M. Vilarinho, A. Singh, *J. Electron. Mater.* **47**(7), 3678–3684 (2018)
35. V. Mata, A. Maldonado, M. de la L. Olvera, *Mater. Sci. Semicon. Process.* **75**, 288 (2018)
36. A. Djelloul, Y. Larbah, M. Adnane, B. Labdelli, M. Ziane, A. Manseri, A. Messaoud, *J. Nano-Electron. Phys.* **10**(2), 02036 (2018)
37. X. Zhao, J. Cheng, *J. Mater. Sci.* **27**(3), 2676 (2016)
38. S. Jongthammanurak, M. Witana, T. Cheawkul, C. Thanachayanont, *Mater. Sci. Semicon. Process.* **16**(3), 625 (2013)
39. H.L. Ma, Z.W. Liu, D.C. Zeng, M.L. Zhong, H.Y. Yu, E. Mikmekova, *Appl. Surf. Sci.* **283**, 1006 (2013)
40. H.-J. Jeon, S.-G. Lee, K.-S. Shin, S.-W. Kim, J.-S. Park, *J. Alloy. Compd.* **614**, 244 (2014)
41. H. Tanoue, M. Takenouchi, T. Yamashita, S. Wada, Z. Yatabe, S. Nagaoka, Y. Naka, Y. Nakamura, *Phys. Status Solidi A* **214**(3), 1600603 (2017)

42. U. Kazuyuki, Y. Yuichiro, T. Ichiro, *Appl. Phys. Express* **10**(1), 015502 (2017)
43. F. Ynineb, N. Attaf, M.S. Aida, J. Bougdira, Y. Bouznit, H. Rinnert, *Thin Solid Films* **628**, 36 (2017)
44. X. Gao, X. Li, W. Yu, *Thin Solid Films* **484**(1–2), 160 (2005)
45. G. Kenanakis, N. Katsarakis, *Mater. Res. Bull.* **60**, 752 (2014)
46. J.C. Vigié, J. Spitz, *J. Electrochem. Soc.* **122**(4), 3 (1975)
47. Y. Lee, H. Kim, Y. Roh, *Jpn. J. Appl. Phys.* **40**(4R), 2423 (2001)
48. J. Cheng, R. Hu, Q. Wang, C.X. Zhang, Z. Xie, Z.W. Long, X. Yang, L. Li, *Int. J. Photoenergy* **2015**, 8 (2015)
49. M. Zirak, O. Moradlou, M. Bayati, Y. Nien, A. Moshfegh, *Appl. Surf. Sci.* **273**, 391 (2013)
50. X.Y. Zhao, B.C. Zheng, C.Z. Li, *J. Inorg. Mater.* **11**, 611 (1996)
51. S.-H. Hu, Y.-C. Chen, C.-C. Hwang, C.-H. Peng, D.-C. Gong, *J. Alloy. Compd.* **500**(2), L17 (2010)